Journal of Nuclear Materials 568 (2022) 153880

Contents lists available at ScienceDirect

Journal of Nuclear Materials

journal homepage: www.elsevier.com/locate/jnucmat

Dopant effect on the spent fuel matrix dissolution of new advanced fuels: Cr-doped UO_2 and Cr/Al-doped UO_2

N. Rodríguez-Villagra[a], O. Riba[b,*], A. Milena-Pérez[a], J. Cobos[a], L. Jimenez-Bonales[a], S. Fernández-Carretero[a], E. Coene[b], O. Silva[b], L. Duro[b]

[a] Centro de Investigaciones Energéticas, Medioambientales y Tecnológicas (CIEMAT). Avda. Complutense 40, Madrid 28040, Spain
[b] Amphos 21 Consulting SL, C/Venezuela, 103, 2da planta, Barcelona 08019, Spain

ARTICLE INFO

Article history:
Received 24 February 2022
Revised 16 June 2022
Accepted 20 June 2022
Available online 21 June 2022

Keywords:
UO_2
Leaching experiments
Deep geological repository
Chromium
Doping
Chromium-doped UO_2

ABSTRACT

To improve the fundamental understanding of the processes controlling spent fuel alteration under deep geological conditions, the influence of dopants (Cr and Cr/Al) on UO_2 matrix stability is evaluated for "modern" types of light water reactor (LWR) fuels with additives. The uranium dissolution behavior of as-prepared 0.06 wt%Cr and 0.05 wt%Cr/0.02 wt%Al doped UO_2 pellets is studied in simplified groundwater containing 19 mM HCO_3^- in autoclaves under hydrogen atmosphere. Sintered disks were exposed to simulated highly carbonated conditions, representative of a repository scenario of water intrusion after a hypothetical canister failure. The uranium concentration released was $\sim 10^{-7}$ M for the 0.05 wt%Cr/0.02 wt%Al doped UO_2 pellet and $\sim 10^{-6}$ M for 0.06 wt%Cr doped UO_2 pellets, after 170 days. The results indicate that the amount of dissolved uranium is slightly lower compared to previous studies in absence of a reductant gas phase, but clearly above the solubility of UO_2(am, hyd). The initial measured pH was 8.9 ± 0.1, which gradually approached a constant value of ~9.2 ± 0.1. Solid characterization at the end of the dissolution experiment, by SEM, Raman spectroscopy and XRD shows that the surface of all pellets remains almost unaltered. The experimental results indicate a potential oxidative dissolution of UO_2, which could be attributed to the presence/intrusion of dissolved oxygen in the prepared synthetic groundwater. In order to identify the mechanism of uranium release, the datasets from the batch experiments are simulated with a PHREEQC model previously calibrated with results of existing spent fuel UOx leaching experiments. The model includes the geochemical processes that are relevant for the studied experimental conditions: (i) non-oxidative dissolution of UO_2, (ii) UO_2 oxidation with O_2, (iii) dissolution of U(VI) by carbonate water, (iv) reduction of oxidized U(VI) on the surface pellet by activated H_2. The ability to activate the dissolved H_2 is studied by implementing a kinetically controlled process of H_2 activation on the Cr surface in the model.

1. Introduction

The safety assessment of deep geological disposal of spent nuclear fuel (SNF) requires a fundamental understanding of the processes controlling fuel alteration and the release of radionuclides into the geosphere. Radionuclide decay is a long-term occurring phenomenon, which may impact the life of future generations. Extensive work has been devoted to conventional UO_2 fuel stability under representative conditions of a Deep Geological Repository (DGR). In recent years, Accident Tolerant Fuels (ATF) types for light water reactors (LWR) have been developed to extend power output and control in operating nuclear reactors and enhancing the accident tolerance in commercial nuclear power plants [1–4]. In the attempt to optimize reactor operation and increase energy production efficiency, the nuclear energy industry is continuously developing new types of fuels. The use of mixed oxide (MOX) fuel has become frequent in the past years, as well as Gd_2O_3-doped UO_2 [5,6]. More recently, the addition of Cr_2O_3 and (Cr_2O_3+Al_2O_3) to UO_2 fuel matrix has been considered to modulate the microstructure triggering grain growth during sintering of the UO_2 pellets and minimizing Fission Gas Release (FGR) [7,8]. This will essentially lower the PCI (Pellet-Cladding Interaction) inside the fuel rods, allowing higher "burnups" than traditional UO_2 fuel. While doped fuels imply an in-reactor performance improvement (in the sense of safety, competitiveness, and economics) [9], it is not known whether the dissolution behavior of such fuels in a DGR environment is the same as for standard fuel. The incorporation of dopants might affect the electrochemical properties of the

* Corresponding author.
E-mail address: olga.riba@amphos21.com (O. Riba).

https://doi.org/10.1016/j.jnucmat.2022.153880
0022-3115/

matrix and, as a consequence, the corrosion rate of the spent fuel matrix [10,11]. The assessment of the expected corrosion behavior should be based on existing characterization and experimental data as well as accurate extrapolations of that data by modelling and numerical simulations. Therefore, it is essential to evaluate the effect of dopants on the matrix corrosion of ATF experimentally through leaching experiments. Alteration mechanisms, potential weaknesses and uncertainties should also be quantified considering the laboratory scale limitations. The resulting evaluations may then be used to scale up and demonstrate long-term safety of ATF in DGR. This study targets two new promising fuel candidates: Cr and Cr/Al-doped UO_2 sample pellets. Both types of fuels are already licensed in some light water reactors, and their use is foreseen to grow and maximize the energy production.

A first evaluation of the behavior of this type of fuels was performed in the FIRST-Nuclides European project [12], which included leaching experiments with fuel containing Cr and Al. These experiments were conducted in parallel to experiments using standard fuel (i.e., without additives). The doped fuel showed a lower release of I and Cs than the standard fuel [13,14]. However, other elements such as Mo and Tc, seemed to have a larger IRF than the standard fuel [15].

The lack of data on the long-term behavior of oxide fuels containing additives becomes an important issue to obtain dissolution data of these fuels and to correlate to that of conventional UO_2 fuels under geological storage conditions. Besides, it is also important to mechanistically determine the Cr and Cr/Al effect on the matrix dissolution. Because of the above, doped fuels have been extensively studied in the framework of the DisCo European project (H2020 European Commission Program) [16], focuses, among other issues, on the development and application of kinetic models to provide the basis for understanding and predict the behavior of spent nuclear fuel, particularly the so-called "modern" fuels, i.e. fuels doped with alumina/chromia, at definitive disposal conditions.

To overcome the inherent complexity of spent fuel corrosion and to identify the effect of the Cr/Al dopants on the UO_2 matrix individually, the present study focused on a prototype material: unirradiated Cr and Cr/Al-doped UO_2 pellets. To understand the effects that adding Cr- or Al-oxide into the fuel matrix would have on SNF dissolution behavior under repository conditions, these materials are studied in experiments using a bicarbonate solution. This enhances the dissolution of uranium, facilitated by the formation of soluble complexes, thus avoiding secondary phase precipitation [17]. The experiments are also performed under H_2 pressure to simulate the reducing conditions in DGR caused by iron corrosion.

2. Materials and methods

2.1. Samples preparation and fabrication procedure

The starting powders used in the experiments were UO_2, Cr_2O_3 and Al_2O_3. The first one was provided by ENUSA and the others by Alfa-Aesar. These materials were characterized by the following tests: (i) measurement of the particle size distribution (Laser Diffraction- Malvern, Series 2600); (ii) morphology of the particles and agglomerates by SEM (TM4000 Plus SEM by HITACHI); (iii) the BET Specific Surface Area (SSA) with N_2 (ASAP 2020 Micromeritics); (iv) evaluation of the purity and the crystalline structure by both XRD (Bruker D8 Advance Eco diffractometer using Cu Kα radiation λ = 1.54056 Å with a Bragg-Brentano configuration at 40 kV and 25 mA); and (v) Raman spectroscopy (Horiba LabRam HR evolution spectrometer, Jobin Yvon Technology, using a He-Ne laser with wavelength equal to 632.8 nm equipped with an Olympus BX41 microscope). The methodology applied for disks fabrication was “dry route” from powders, pressing and sintering [18]. Prior to that, natural UO_2 was thermally treated in a 4.7%H_2-N_2 atmosphere at 1100°C to attain stoichiometric $UO_{2.0}$. These powders were mixed in weighted proportions with 1wt% of Ethyl Bis Stearamide ($C_{38}H_{76}N_2O_2$), EBS, supplied by Tokyo Chemical Industry. This molecule has been selected as binder and lubricant due to its higher percentage of recovery of the mixing powders [19] and to guarantee the integrity of the pellets [20] Low-energy ball milling has been used to ensure suitable homogenization. The fabrication process is described in detail in [18,21]. As a result, 0.06 wt% Cr_2O_3, and 0.05 wt% Cr_2O_3/0.02 wt% Al_2O_3 doped UO_2 samples were obtained. For the sake of comparison, pure UO_2 pellets were prepared following the same methodology. The results of raw powder characterization, prior to the sintering of the samples, can be seen in Table 1. The same characterization methods were also used for surface analysis of prepared pellets, shown in Section 3.1. Prior to microstructural characterization, samples were properly prepared by following a conventional metallographic sequence of grinding and polishing down to 3 μm by using a monocrystalline diamond suspension (provided by BUEHLER, Inc.) and thermally etched at 90% of the sintering temperature in order to reveal the grain structure.

Table 1
Parameters of raw material characterization: calculated structural data (a, b and c) from Rietveld refinement with the error in the last digit (number in parentheses); and the BET SSA with N_2 (SSA errors are increased by a factor of 10–15% based on propagation of analytical uncertainties).

Sample	Lattice parameter / nm	SSA (BET) /$m^2 \cdot g^{-1}$
UO_2	a = b = c = 0.546920(4)	0.95 ± 0.02
Al_2O_3	a = 0.7944(6); b = 0.7980(4); c = 1.1722(6)	37.6 ± 0.4
Cr_2O_3	a = b = 0.49586(7); c = 1.3592(2)	3.47 ± 0.02

Table 2
Composition of the synthetic aqueous media representing groundwater with high bicarbonate content (uncertainty in analytical measurements below 15%).

Conc / mol·l $^{-1}$	Bicarbonate solution, BC
Na	$2.1 \cdot 10^{-2}$
Al	$3.55 \cdot 10^{-9}$
Cr	$4 \cdot 10^{-9}$
Fe	$9 \cdot 10^{-8}$
U	$3.6 \cdot 10^{-9}$
HCO_3^-	0.0193
Cl^-	$1.1 \cdot 10^{-3}$
SO_4^{2-}	$3.3 \cdot 10^{-5}$
pH	8.9 ± 0.1
Eh / V	0.06 ± 0.03
Alkalinity /meq·l^{-1}	19.4

The high bicarbonated solution (abbreviated as BC: 19mM $NaHCO_3$ + 1 mM NaCl) was carefully prepared by the addition of pure chemical reagents: $NaHCO_3$ (VWR,NORMAPURE, 99%) and NaCl (VWR, SUPRAPURE, 99.99%) to boiled and cooled MilliQ water and bubbling He gas to take out dissolved O_2 and minimize the uptake of atmospheric O_2 and CO_2. The solutions inside polypropylene screw capped bottles jars with polypropylene screw closure have been stored in an Ar atmosphere glove box for more than one month (1–8 ppm O_2 and 20-25.3 °C during storage in the same glove box than experiments were run), and then filtered by means of a PVDF membrane with a pore size of 0.22 µm. Further details about the simulated water composition measured by ICP-MS (Thermo Fischer Sci ICAP-Qc with QCell and KED modes) are shown in Table 2.

2.2. Leaching experiments

The detailed description of the experimental procedure is published in [22]. Briefly, for setting up the dissolution experiments,

Fig. 1. Image of PEEK-lined stainless steel autoclaves at CIEMAT radioactive facilities.

the pellets shaped as a disk of approximately 1 g (1.7 mm in height and 9.6 mm in diameter), fabricated as described in Section 2.1, were exposed to 300 ml of BC water at pH 8.9 ± 0.1 and under 6–8 bar of 4.7%H_2/N_2 atmosphere during 168 days and 22 ± 3 °C. All static dissolution experiments with doped UO_2, were performed in an Ar glove box in autoclaves (Fig. 1) with a Pt wire, in which sample disk was suspended. PEEK-lined 316 stainless steel autoclaves (total volume 380 ml; Fig. 1) were equipped with a PEEK vessel and three valves in the lid (quick-fit type) to allow injecting/releasing gas into the reactor and sampling of solutions during the experiment. In our dissolution experiments, oxygen level immediately before the start was reducing/anoxic (O_2 < 2 ppm) and during the experimental time the final oxygen concentration measured raised to 1000 ppm. The O_2 concentration in the glove box was monitored by means of an MB-OX-SE1 oxygen analyzer (MBraun) of ZrO_2 with a measuring range of 0–1000 ppm. Due to the reactor overpressure, aliquots of aqueous phase (3.3–3.7 ml) were collected through a sampling valve without opening the reactor at specific time intervals using ICP-MS to quantify the elemental release to water (U, Cr, Al), without any replenishment of aqueous phase but refilling with gaseous phase in order to maintain pressure levels. Then, autoclaves were refilled with 4.7%H_2/N_2 until the pressure increased up to 8 bar. The pH and redox values were measured *ex-situ*. At the end of the dissolution experiments, the test vessels were rinsed with 300 ml 2M HNO_3(aq), which were maintained for 24 h in the vessel to determine the fraction adsorbed (colloidal or precipitated material) on the walls. The rinse solutions were collected and also measured by ICP-MS.

Microfiltered (GHP Acrodisc, PALL, 0.2 µm) and ultrafiltered (Amicon Ultra-4 3k de Millipore, < 2 nm) samples were measured by ICP-MS to quantify dissolved U and Cr concentrations (intrinsic uncertainty ± 15%). Both, Limit Of Detection (LOD) and Quantification (LOQ) for leachant, defined respectively as the lowest concentration that produces a detectable signal and the minimum quantifiable level with acceptable accuracy under certain conditions. 10 blank replicates (BC solution) are run by ICP-MS and the standard deviation (STD) is determined. Both parameters were quantified as follows: LOD = 3 x STD and LOQ = 10 x STD.

2.3. Model description

The batch model applied for the simulation of the present leaching experiments is based on the geochemical processes considered in the 1D reactive transport model of [23]. The geochemical code PHREEQC v.3.6.2 [24] coupled with the ThermoChimie v.10a database [25], is used to simulate the experimental data. Based on the experimental set up, the following considerations were taken into account:

- The simulations of the two leaching experiments consider a leachant (bicarbonate water) that is equilibrated with 1000 ppm of O_2, in agreement with the final measured O_2 concentration in the glove box, as specified in Section 2.2.
- The kinetic reactions at the surface of the pellets were: the oxidation of UO_2 surface by O_2 and dissolution of the oxidized surface by complexation with H_2O and carbonate.
- Potential activation of H_2 (hydrogen partial pressure of 0.37 atm) on Cr surface and the subsequent reduction of oxidized uranium on the surface was considered in the simulation of both experiments.
- The kinetic constant for the activation of H_2 on Cr_2O_3 was 10^{-6} m·s^{-1}, which represents a diffusion-controlled process that was determined in [26] for the H_2 activation with palladium.
- The surface area / volume solution ratio considered for simulating the oxygen oxidation rate and UO_3 reduction was calculated from the geometry of the pellet assuming a roughness factor of 3.5 [27]. The upper limit of the roughness factor, 9, was also considered in the simulations [27].
- The surface area / volume solution ratio considered in the activation of H_2 with Cr_2O_3 was calculated with the % in weight of Cr_2O_3 contained in the pellets.
- A surface site density of $1.76{\cdot}10^{-4}$ mol·m^{-2} UO_2 was considered in simulations. This value was experimentally determined from the maximum Cs sorption on the UO_2 surface [28,29] and is close to the value calculated by Clarens et al. [30].

3. Results and discussion

3.1. Solid characterization

To perform the characterization of sintered samples, the obtained specimens were polished and thermally etched (95% of sintered temperature). Doped sample characterization was carried out by XRD and Raman spectroscopy to verify the final stoichiometry, and by SEM-EDX to analyze the microstructure and the grain size distribution. The specific surface area was determined by the BET method and the density was geometrically calculated.

Fig. 2 shows the grain microstructure of representative sintered pellets by SEM: A) UO_2, B) 0.06 wt% Cr_2O_3-UO_2 and C) 0.05 wt%Cr_2O_3/0.02 wt%Al_2O_3 -UO_2. Microstructural examination of the grain growth in doped-UO_2 also reveals that the U mixed oxides containing Cr and Cr-Al samples show a homogeneous microstructure of well solubilized dopants in solid solution. Also, no segregated phases are found by XRD (Fig. 3) and Raman spectroscopy (Fig. 4). This indicates that dopants are dissolved into the UO_2 grains.

Fig. 3 displays the diffraction patterns obtained from the 0.06 wt% Cr_2O_3-UO_2 and 0.05 wt% Cr_2O_3/0.02 wt% Al_2O_3-UO_2, in comparison with pure UO_2. It is well-known that the crystal structure of UO_2 is cubic, fluorite-type, so the lattice is characterized by only one lattice parameter (a). Diffraction peaks of all prepared

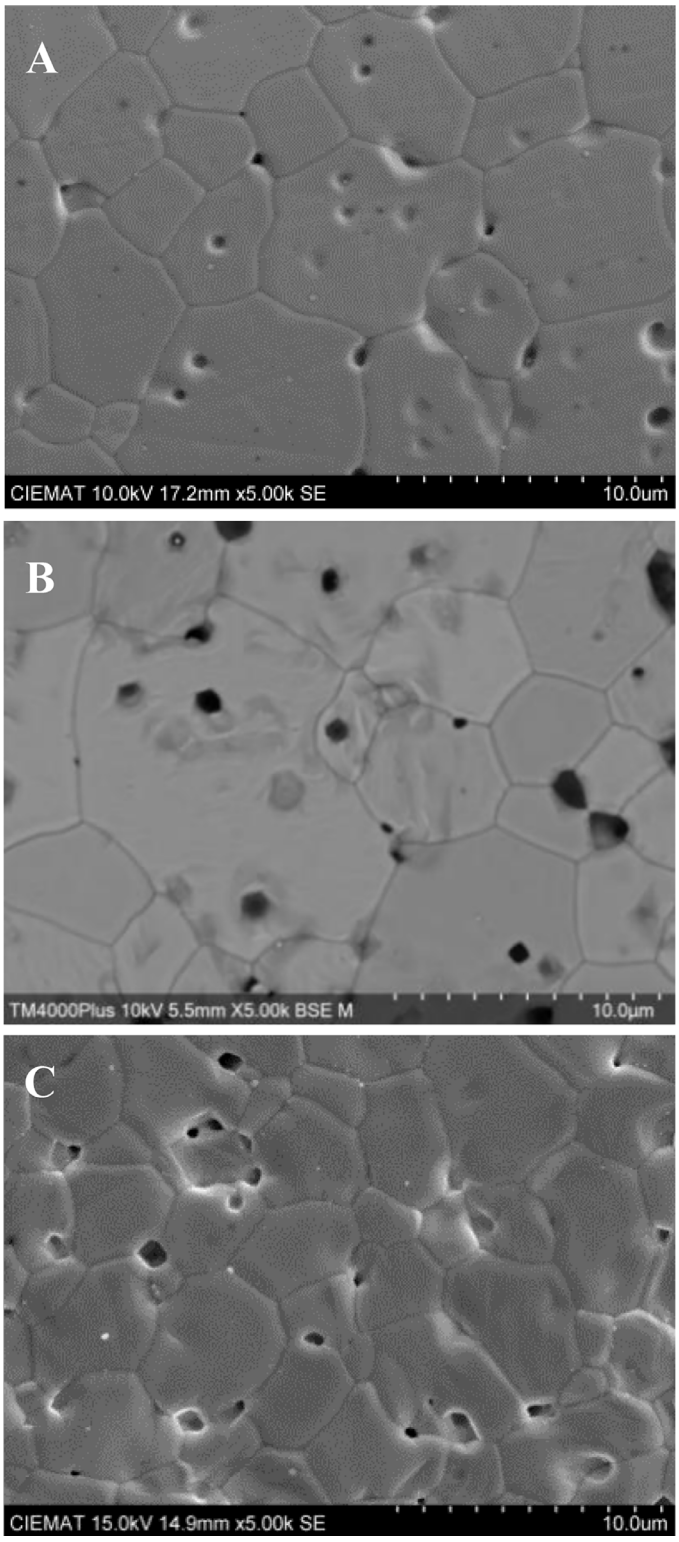

Fig. 2. Microstructure images of A) pure UO_2; B) 0.06 wt% Cr_2O_3-UO_2 and C) 0.05 wt%Cr_2O_3/0.02 wt%Al_2O_3 -UO_2.

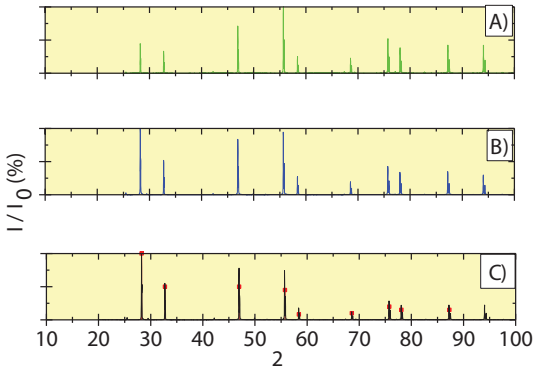

Fig. 3. XRD patterns of fabricated solid samples 0.06 wt% Cr_2O_3-UO_2 (A) and 0.05 wt% Cr_2O_3/0.02 wt% Al_2O_3-UO_2 (B) - compared to pure UO_2 pellet (C) and UO_2 ICDD 00-041-1422 - UO_2 reference data as red dots (on C).

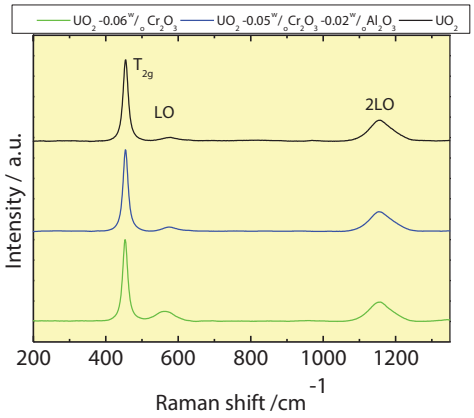

Fig. 4. Raman spectra of fresh doped UO_2 pellets. Band 445 cm^{-1} corresponds to the vibration of the U–O bond in the UO_2 matrix, band 575 cm^{-1} represents the defects of the UO_2 lattice and band at 1145 cm^{-1} shows the first overtone of this phonon vibration.

samples were acquired under the same conditions, and the lattice parameter *a* was obtained by using the unit cell refinement method, applying the corresponding error corrections. From the diffraction peaks of each sample, it can be seen that dopants are well dissolved into UO_2 grains. XRD diffraction patterns of Cr- and Cr/Al- doped UO_2 samples show a slight decrease of the lattice parameter with respect to undoped UO_2, which demonstrates that dopants have entered in the UO_2 fluorite structure [11,18,31,32].

Fig. 4 illustrates Raman spectra acquired for the initial samples. The plot represents the averaged spectra from 10 individual spectrums recorded at various locations of each disc. No oxidation on doped-UO_2 is observed in preleached samples by XRD and Raman confirming the stoichiometric conditions at the beginning of the experiments.

The Raman spectroscopy results (see Fig. 4 bottom) show the classic bands and features described in the literature [33–35]. Based on the profile analysis (curve fitting) of peaks, three main bands were identified, whose wavenumbers have been calculated from the second derivative analysis. The band at 445 cm^{-1} is assigned to the T_{2g} (vibration of the U–O bond in the UO_2 matrix). The band at 575 cm^{-1} is due to the LO phonon and is associated with the close to perfect fluorite lattice. The band at ~1145 cm^{-1} is assigned to a phonon vibration of the lattice, which causes the 2LO band (the first overtone of this phonon vibration).

By using this second derivative method, the specific corresponding Raman shifts of materials shown in Table 3 are obtained.

The analysis of the normalized areas has been performed taking the T_{2g} band as a reference. The ratio between the LO band area with respect to that of the T_{2g} band shows an increase with the Cr concentration. As shown in Table 4, the increase in the normalized area ALO/AT_{2g} with doped samples demonstrates the effect of the dopants distorting the lattice, as this Raman feature is related with the presence of defects in the structure [18]. In addition, this

Table 3
List of the different vibrational modes featured in the Raman spectrum of as-prepared doped UO_2 solid samples.

Raman mode assigned	UO_2 Experimental Raman shifts /cm^{-1}	0.06 wt% Cr_2O_3-UO_2	0.05 wt% Cr_2O_3/0.02 wt% Al_2O_3-UO_2
T_{2g}	446.5 ± 0.4	445.2 ± 0.6	441.5 ± 0.6
LO	568. 1 ± 1.7	567.0 ± 2.3	562.2 ± 1.9
2LO	1145.1 ± 0.8	1146.0 ± 1.2	1142.0 ± 1.7

Table 4
Parameters of Cr- and Cr/Al-doped UO_2 pellets used in the described leaching experiment. Areas are normalized by the area of T_{2g} (SSA errors are increased by a factor of 10–15% based on propagation of analytical uncertainties).

Sample / wt%	Lattice parameter *a* / nm	Raman norm. area LO/T_{2g}	Raman norm. area 2LO/T_{2g}	SSA (BET) / $m^2 \cdot g^{-1}$	Density geom./ $g \cdot cm^{-3}$	Grain size / μm
UO_2	0.547260(9)	0.05 ± 0.01	1.27 ± 0.03	0.36 ± 0.01	8.27 ± 1.15	6.55 ± 1.03
0.06wt% Cr_2O_3-UO_2	0.547113(7)	0.15 ± 0.03	1.01 ± 0.14	0.63 ± 0.02	9.83 ± 0.07	10.16 ± 1.17
0.05wt% Cr_2O_3/0.02wt% Al_2O_3-UO_2	0.547198(5)	0.10 ± 0.03	1.07 ± 0.20	0.25 ± 0.01	9.80 ± 0.43	9.87 ± 1.02

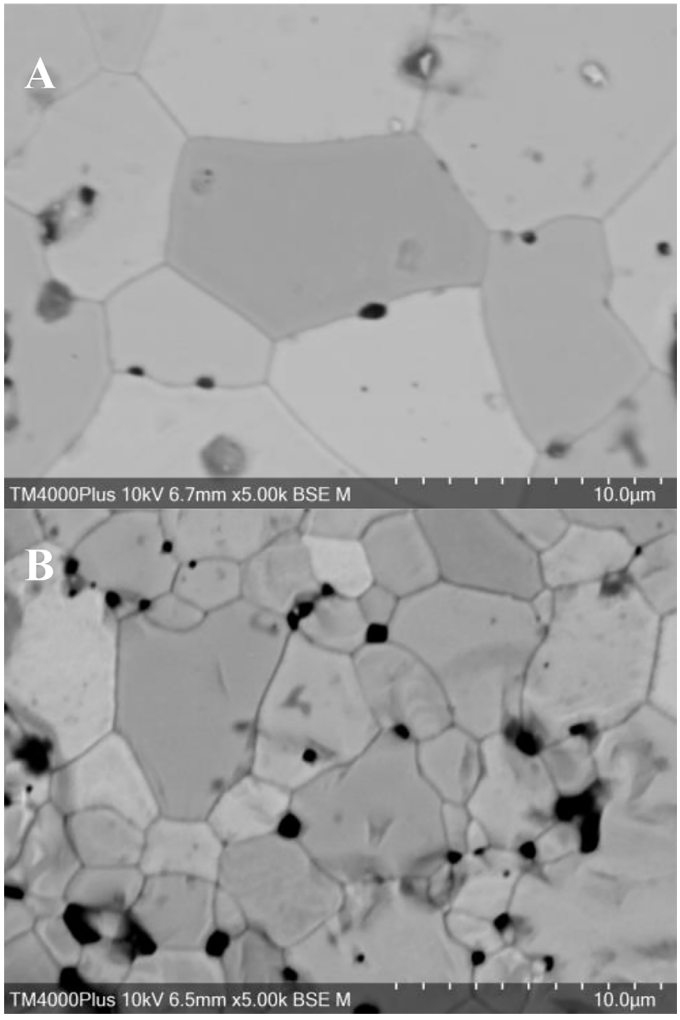

Fig. 5. SEM micrographs from the leached samples in BC of A) 0.06 wt% Cr_2O_3-UO_2 and B) 0.05 wt% Cr_2O_3/0.02 wt% Al_2O_3-UO_2 after dissolution experiments.

behavior is confirmed by the decrease of the area A2LO/AT_{2g}, as both bands are related with the fluorite-type lattice of UO_2. These results are summarized in Table 4 and considered as the basis to define the solids that were leached (see Section 3.3). The average grain size was determined by taking SEM images (Fig. 2) using the linear intercept method as described in the ASTM standards [36] and taking into account at least 500 grains. Uncertainties of the grain sizes were calculated in terms of the standard deviation and error propagation. Data for an undoped UO_2 sample prepared according to the same procedure as the doped samples are given in Table 4 for comparison. As a result, doping with Cr_2O_3 or Cr_2O_3/Al_2O_3, increases the average grain sizes and densities in comparison with pure UO_2

The characterization of the UO_2 and doped-UO_2 pellets indicates the formation of a single and pure phase free of hyperstoichiometric surface oxidation. The pure UO_2 reference pellet, prepared by our synthesis route (Fig. 2.A and Table 4) exhibits a microstructure with an equiaxial grain shape, an average grain size of 6.55 μm, and a uniform grain size distribution. Small pores were observed and mainly located at grain boundaries triple points, but also within grains. In contrast, the grains of the Cr- and Cr/Al-doped UO_2 were noticeably larger, with average grain sizes of around 10 μm (Fig. 2. B and C, and Table 4), although the overall grains shape and porosity distribution was similar.

3.2. Post-leached solid characterization

SEM, XRD and Raman measurements on pellets after the dissolution experiments complement the picture of data obtained (Fig. 5 for SEM; Figs. 6, 7 and Table 5 for XRD and Raman results).

Fig. 5 shows the grain structure of sintered and leached pellets. No precipitates or segregation are observed in any sample, meaning that dopants are well solubilized. The comparison between SEM micrographs of the disks before (Fig. 2) and after leaching (Fig. 5) indicates that no significant precipitation of secondary hydrated phases has occurred, compatible with carbonate aqueous systems that stabilize the U(VI) in solution [37–39]. Any trace of solubilized U may presumably remain in solution assisted by complexing anionic agents such as carbonates. This and the level of measured U concentrations in solution, confirms the stability of the doped UO_2 matrix under these specific conditions.

The lack of precipitated, secondary phases containing U is also confirmed by XRD and Raman results, shown in Fig. 6, Fig. 7 and Table 5, as expected in presence of carbonates that inhibit solid formation at pH above 8.5, because these complexing ligands solubilize U(VI) by forming highly stable complexes in solution [39]. The only presence of an amorphous phase around 18.8 (°2θ) well-matched with $Al(OH)_3$ in a proportion below 5% was identified by XRD in the leached sample UO_2 doped with 0.05wt% Cr_2O_3 – 0.02 wt% Al_2O_3, as a broad peak (Fig. 6.b). This amorphous phase was not observed on the non-leached sample (Fig. 3), hence we presume that it is associated with the leaching process.

Table 5
Analysis of the results obtained from the analysis by XRD and Raman spectroscopy of the doped UO2 samples after leaching in BC solution. Areas are normalized by the area of T_{2g}.

	XRD	Raman shift assigned to Raman mode			Raman normalized area	
Sample / wt%	Lattice parameter *a*/ nm	T_{2g} (cm^{-1})	LO (cm^{-1})	2LO (cm^{-1})	LO/T_{2g}	$2LO/T_{2g}$
0.06wt% Cr_2O_3-UO_2	0.5470419(8)	448.3 ± 0.7	571.4 ± 1.1	1148.4 ± 0.9	0.18 ± 0.06	0.92 ± 0.15
0.05 wt% Cr_2O_3/0.02 wt% Al_2O_3-UO_2-	0.5470803(8)	445.7 ± 0.6	569.9 ± 1.2	1145.4 ± 1.3	0.08 ± 0.02	0.69 ± 0.05

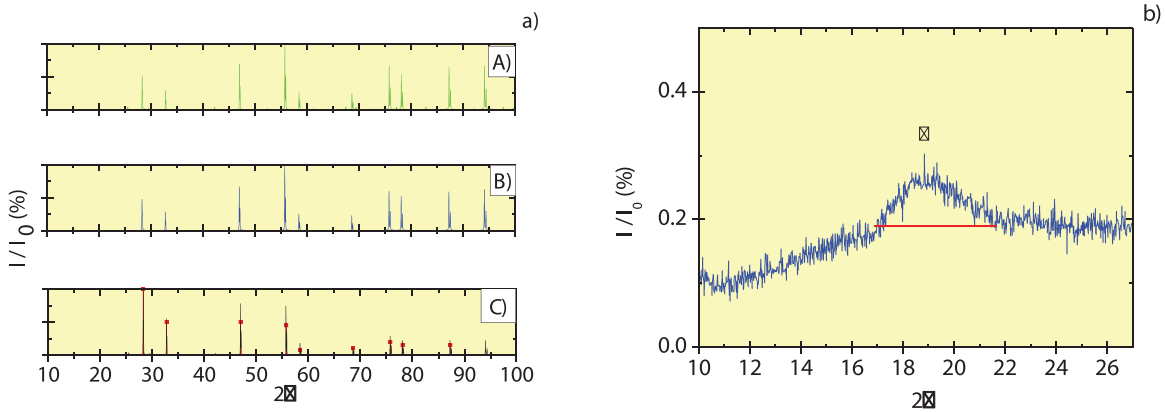

Fig. 6. Post-leaching solid characterization by XRD from leaching experiments in BC system done for (a. A) UO_2 doped with 0.06 wt% Cr_2O_3 and (a.B) UO_2 doped with 0.05wt% Cr_2O_3 – 0.02 wt% Al_2O_3 compared to pure and non-leached UO_2 pellet and UO_2 ICDD 00-041-1422 - UO_2 reference data (a.C); and (b) corresponds to a low angle detail of precipitated $Al(OH)_3$ (am) with a characteristic amorphous peak observed in the leached sample UO_2 doped with 0.05 wt% Cr_2O_3 – 0.02 wt% Al_2O_3.

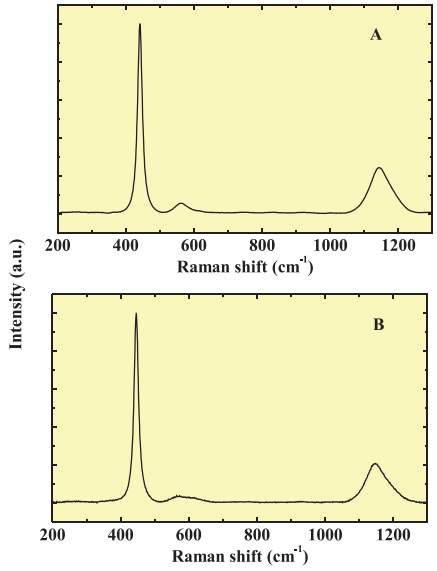

Fig. 7. Post-leaching solid characterization by Raman spectroscopy from leaching experiments in BC system done for (A) UO_2 doped with 0.06 wt% Cr_2O_3 and (B) UO_2 doped with 0.05 wt% Cr_2O_3 – 0.02 wt% Al_2O_3.

A comparison of both data, Raman shift of the main bands and normalized areas, in samples before (Tables 3 and 4) and after (Table 5) leaching experiments can be explained as a growth of the defects band (LO band) and a decrease the 2LO band, as a result of leaching. These changes are insignificant, since uncertainties overlap for both, Raman shift of 3 cm^{-1} and normalized areas.

In conclusion, leaching fresh doped-UO_2 solid samples in a simplified geochemical environment such as bicarbonate water did not apparently influence the evolution of the microstructure on the fuel surface and on the grain boundaries.

3.3. Leaching experiments

The maximum pressure in the autoclaves was limited to 8 bar of 4.7%H_2/N_2 during 168 days; however a slight loss of pressure was observed between sampling time, where minimum value was 6 bar that means an allowable pressure loss of 25% and a leak rate of ~0.04 bar per hour. Once that minimum value of 6 bar was reached, autoclaves were refilled with reducing gas until the pressure increased up to 8 bar. Therefore, the change of pressure to which the samples are exposed may have disturbed the system and then, may have impact the measured concentration and pH values, especially the redox potentials.

Fig. 8 shows the temporal evolution of uranium concentration in the leaching experiment for Cr doped UO_2 and Cr/Al-doped UO_2. Filled symbols represent microfiltered aqueous samples and empty symbols are ultrafiltered. The U concentration in the solutions, displays different patterns for the two studied systems. While for Cr/Al-doped UO_2, the uranium concentration rapidly reaches a plateau and after 10 days of reaction the uranium concentration is ~10^{-7} M, with Cr-doped UO_2, the uranium concentration keeps increasing until 119 days' reaction time, stabilizing at a value of ~10^{-6} M for the three last dissolution points (we cannot verify if this trend continues afterwards). In both systems, measured U concentrations are typically representative for oxidizing conditions in carbonate systems [40] with concentrations higher than those characteristic of U(IV)(aq) in equilibrium with $UO_2{\cdot}H_2O$ (am) [15,41–48]. In most cases, the U concentration in the ultrafiltered samples represents more than 80% of the total U concentration (filtered), the difference corresponds to the uncertainty of measurement ICP-MS technique (±15%). The presence of any U-colloids, *i.e.* difference between total and ultrafiltered U concentrations, larger than 2 nm is discarded after 168 days in both, the Cr- and Cr/Al-UO_2 systems. The fact that the H_2 does not lead to reducing conditions agrees with the slow activation kinetics of this agent. Several studies explaining the hydrogen effect on the corrosion of spent

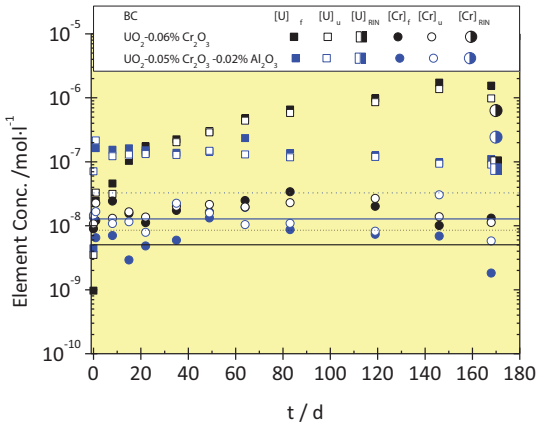

Fig. 8. Autoclave concentrations of ^{238}U and Cr as function of time, represented as symbols. Squares represent data of ^{238}U concentration from UO_2 doped with 0.06wt% Cr_2O_3 (in black color) and from UO_2 doped with 0.05 wt% Cr_2O_3 – 0.02 wt% Al_2O_3 (in blue color). Circles represent data of Cr concentration from UO_2 doped with 0.06 wt% Cr_2O_3 (in black color) and from UO_2 doped with 0.05wt% Cr_2O_3 – 0.02 wt% Al_2O_3 (in blue color). Filled symbols represent filtered and empty symbols are ultrafiltered analyzed solutions. Solid and dotted lines in blue and black corresponds to Limit Of Quantification and Limit Of Detection of Cr and U respectively (LOQ (Cr) = $3{\cdot}10^{-8}$ M; LOD (Cr) = $1{\cdot}10^{-8}$ M; LOQ (U) = $8{\cdot}10^{-9}$ M; LOD (U) = $5{\cdot}10^{-9}$ M). Rinse values are included.

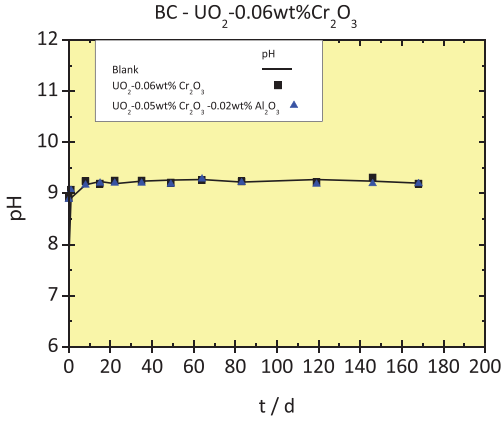

Fig. 9. Measured pH from leaching experiments using a BC leaching solution. Black line corresponds to the blank test, squares represent data of UO_2 doped with 0.06 wt% Cr_2O_3 and triangles represent data of UO_2 doped with 0.05 wt% Cr_2O_3 – 0.02 wt% Al_2O_3.

fuel have shown the need of metallic particles, present in spent nuclear fuel, to act as catalysts for the electron transfer from hydrogen to the fuel matrix [49,50]. Additionally, the solid characterization indicates that the stoichiometry of the solid is close to UO_2, therefore, it can be assumed that the starting material is free from an oxidized layer in the surface. From the above discussed, it is concluded that the presence of hydrogen did not provide the expected reducing conditions and the measured uranium concentration are the result of an oxidative dissolution process at the pellet surface promoted by carbonates acting as complexing agents.

Chromium is a redox-sensitive element, which means that its solubility behavior in aqueous media is mainly affected by redox potential and pH. Thermodynamically, Cr(VI) could only be present at relatively high pH [51]. At low pH, the high redox potential of the Cr(VI)/Cr(III) couple promotes Cr(III) stabilization. In contrast, under alkaline conditions the redox potential is reduced, which points out to a stabilization of Cr(VI). Consequently, Cr(VI) could thermodynamically only exist at relatively high pH (>9) solubilized as chromate feasible in both aerobic and mildly anoxic environments [52]. Chromium released (Fig. 8) is in the solubility range ($\sim 2{\cdot}10^{-8}$ M) [53] knowing that the measured Eh was near zero (not shown) and below the LOQ ($3{\cdot}10^{-8}$ mol·l^{-1}).

Also shown in Fig. 8 are the results of the analysis of the rinse solutions of the leaching vessels. Uranium measured concentrations in the washout solution was around 10^{-7} and $8{\cdot}10^{-8}$ M for the Cr- and Cr/Al-doped UO_2 pellets, respectively. That low concentration values in the vessel rinse analysis of the Cr-doped UO_2 pellets system (< 10% than final U concentration in the leaching experiments) would indicate that almost negligible concentrations of uranium were sorbed on the vessel walls. However, for the Cr/Al-doped UO_2 pellets this fraction represents about 70%. A possible explanation for the amount of adsorbed U observed on the vessel walls in the Cr/Al system could be eventually attributed to U co-precipitation with $Al(OH)_3$, for which the presence could be supported by the precipitation of the Al(OH)3(am) phase as revealed by the XRD analysis (Fig. 6) or maybe partially sorbed as UO_2^{2+}.

The amount of reactive surface area exposed to a given amount of solution is given by the surface area (SA) to solution volume (V) ratio (SA/V). Measuring accurately the reactive surface area of sintered ceramic pellets with high density introduces a certain degree of uncertainty. The SSA measured by Brunauer–Emmett–Teller (BET) method [54], measured by gas (N_2) physisorption, provides an accurate quantification of the surface area to the atomic scale. However, BET tends to overestimate the reactive surface area, taking into account solid features (e.g., cracks or roughness in the surface). As shown in Table 4, measured SSA (BET, N_2) of initial pellets was 0.63 ± 0.02 and 0.25 ± 0.01 m$^2{\cdot}$g^{-1} for Cr- and Cr/Al-doped UO_2 pellets, respectively. Another approach to the surface area from a geometric perspective is calculated by considering pellets as perfect cylinder shape, but this tends to underestimate the surface area due to exclusion of small-scale surface features, adhered fine particles and rough topography. Calculated geometric SSA of both solid samples was 0.0002 m$^2{\cdot}$g^{-1} (without applying any roughness factor). Given the discrepancies that arise between BET measurements and geometric estimation of surface area, initial and final SA/V was estimated by both methods, taking into account the total sampling volume at the end of leaching time and the initial pellet SSA. Thus, considering BET surface area the variation on SA/V was from ~inital 2051 m^{-1} to a final value of 2447 m^{-1} for the Cr-doped UO_2 pellets; and from 790 to 911 m^{-1} for the Cr/Al-doped UO_2 pellets. That values are 3 orders of magnitude times higher than the value estimated by the geometric approach, being in this case the change in SA/V ratio from ~ 0.7 m^{-1} (initial) to ~0.8 m^{-1}(final). In both approaches, the change in SA/V is increased by a factor of ~1.2. Under these static leach conditions, these findings suggest that the potential impact of SA/V may be considered relatively minimum because of the large leachant volumes and then, very low SA/V ratios used in the tests.

The measured pH (uncertainty of ± 0.1) after sampling in the glove box increases from 8.9 during the first 10 days and it is stabilized at around 9.2, independently on the tested material. The same pH is also measured from a blank test (see Fig. 9). From these data, it can be concluded that the measured pH was almost constant during the experiments.

Pre-oxidized U phases were neither detected by XRD and Raman in the prepared pellet nor in the post-leached solid characterization. Therefore, it is reasonable to presume that the oxidizing source, responsible for the U(VI) produced, may be introduced via solution species such as residual dissolved oxygen during the transfer from outside to inside the glove box, or the unforeseen oxygen intrusion in the glove box that may prompt dissolved oxygen in the aqueous solution during its storage time in the glove box before being passed from the glove box to the autoclaves. This hypothesis is based on the fact that even degassed water was conveniently achieved by bubbling with helium to re-

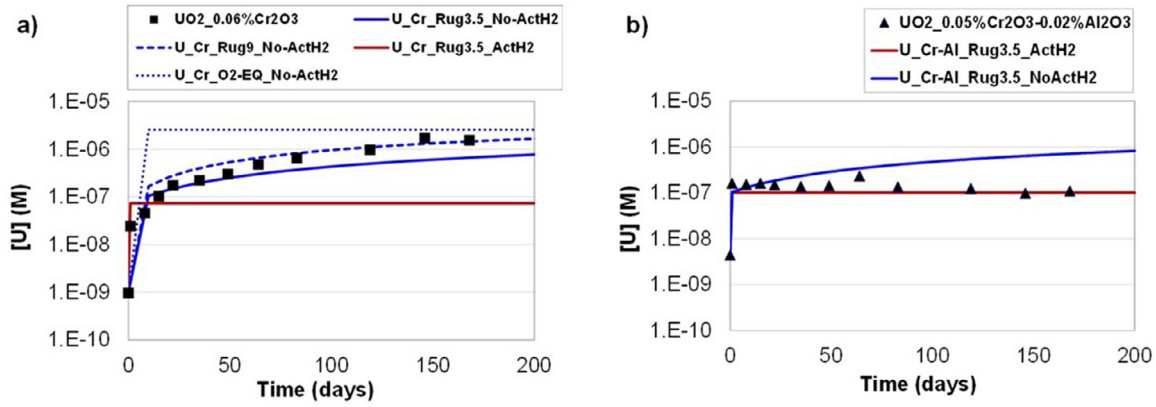

Fig. 10. Experimental aqueous concentrations of 238U as function of time, (symbols) and results of the simulations (lines). (a) 0.06 wt% Cr_2O_3-UO_2 and b) 0.05 wt% Cr_2O_3 – 0.02 wt% Al_2O_3-UO_2. Blue lines represent simulation results with H2 no activated by Cr_2O_3. Red lines represent simulation results with H_2 activated by Cr_2O_3. Solid lines are obtained when using a surface roughness factor of 3.5 [27]. Dashed line represent a surface roughness factor of 9 [27], while dotted line stands for the evolution of the concentration of uranium in solution when UO_2 is oxidized by O_2 according to thermodynamic equilibrium.

move dissolved oxygen, the oxygen will be reabsorbed if there is any contact with air. As mentioned in Section 2.2, for the period of the dissolution tests, the final oxygen concentration measured raised to 1000 ppm. Thus, reducing conditions may not exist in the sealed and pressurized vessels. Under these alkaline conditions (pH 8.9), the measured U concentration is lower for the Cr/Al-doped UO_2 (Fig. 8) over the time range of the experiments when compared to Cr-doped UO_2. Such a decrease could indicate a synergistic effect of Cr_2O_3-Al_2O_3 on the catalytic activation of H_2. From the measured uranium concentration in the rinse samples, no precipitation/sorption is observed anywhere in the system.

The uncertainties in this work are the uncertain redox conditions inside the vessels (measured when samples were taken out of the autoclaves and reaching a measured value Eh of around 0.1 V).

3.4. Simulation results of the experiments

The simulation results are shown in Fig. 10a and b together with the experimental temporal evolution of U from Cr- doped UO_2 and Cr/Al- doped UO_2, respectively. From the model described in [23] and the specific considerations outlined in Section 2.3 of the present article, two types of simulations were performed: with and without H_2 activation. The model results indicate that the concentration of uranium in solution is better described by suppressing the activation of hydrogen when the dopant is Cr_2O_3 (Fig. 10a), while when adding both dopants Cr_2O_3+Al_2O_3, the experimental data is well reproduced by assuming hydrogen is activated by chromia supported on alumina (Fig. 10b).

A simulation assuming that the concentration of uranium in solution is given by the solubility of UO_2 under the oxygen concentration of the autoclave (dotted blue line in Fig. 10a) overestimates the measured uranium levels for short contact times.

The results indicate that when Cr_2O_3 is supported on Al_2O_3 (in the UO_2 doped with 0.05wt% Cr_2O_3 – 0.02 wt% Al_2O_3), chromia can activate H_2, having a similar function as the epsilon particles contained in the irradiated spent fuel and, therefore, limiting the pellet matrix dissolution [55–57]. As supported by both the experimental data and the corresponding simulation, this is not the case in 0.06 wt% Cr_2O_3 doped UO_2, when Cr is the sole dopant. Although not sufficient data are yet available to definitively confirm these conclusions, this outcome agrees with the results on the different catalytic activity of Cr in the oxidative dehydrogenation used in the production of alkenes, that shows that Cr activity is improved when it is supported by other metal oxides such as Al_2O_3 [58–60]. Several studies indicate that when chromia is supported on another metal oxide (e.g. Al_2O_3, TiO_2, SiO_2, ZrO_2, etc.), the structure and reactivity properties are altered by stabilization of Cr different oxidation states (Cr^{3+}, Cr^{5+} and Cr^{6+}) and an improvement in the activity/selectivity of these chromia-based catalysts is observed [61–64].

4. Conclusions

The UO_2-based materials were systematically produced by using industrial metallurgical procedures and were carefully characterized. Specimens were fabricated by homogenizing stoichiometric proportions of UO_2 with a nominal concentration of 0.06 wt%Cr_2O_3 and 0.05 wt%Cr_2O_3/0.02 wt%Al_2O_3 over the UO_2 total mass. Prepared sample pellets were characterized using XRD, Raman spectroscopy and SEM-EDX. Characterization of the synthesized materials confirmed that high density UO_2 was successfully formed. Dissolution experiments of freshly prepared 0.06 wt%Cr_2O_3 and 0.05 wt%Cr_2O_3/0.02wt%Al_2O_3 UO_2 pellets were conducted in bicarbonate water that could be considered as relevant from the interaction between natural barriers (groundwater) and engineering barriers. The effect of H_2 was studied by means of leaching experiments of doped-UO_2 pellets under a 4.7%H_2/N_2 atmosphere. The U and dopants concentration released into the aqueous solution were quantified by ICP-MS. The experimental temporal evolution of uranium concentration was simulated with a spent fuel alteration model [23].

From the results discussed above the following conclusions can be drawn:

- The autoclaves where the experiments have been performed undergo a slight loss of pressure during the duration of the tests.
- Leaching fresh doped-UO_2 solid samples in bicarbonate water did not apparently influence the evolution of the microstructure on the fuel surface and on the grain boundaries.
- The presence of H_2 gas did not provide the expected reducing conditions considering its thermodynamic properties. It slow activation kinetics leads to uranium concentrations corresponding to oxidative dissolution of the pellet surface.
- The U concentration in the solutions show different patterns for the two studied systems: the uranium concentration reaches plateau levels of uranium concentration $\sim 10^{-7}$ M in Cr/Al-doped UO_2 leaching experiments, however, in Cr-doped UO_2 the U concentration increases with time up to uranium concentration $\sim 10^{-6}$ M, after 170 days of reaction time. The effect of carbonate is well established as complexing agent that

enhances the solubilización of U(VI) formed on the surface of the pellet as a result of the oxidation of U(IV). The potential existence of dissolved oxygen (possibly introduced via solution species as residual dissolved oxygen) accelerates the dissolution of U in water that contains complexing ligands.
- The modelling of the leaching data indicates the different behavior of temporal U evolution between UO_2 doped with 0.06 wt% Cr_2O_3 and UO_2 doped with 0.05 wt% Cr_2O_3/ 0.02 wt% Al_2O_3. These differences seem to respond to the fact that Cr_2O_3 supported in Al_2O_3 is able to activate H_2, which is diminished when Cr acts as a sole dopant.

Declaration of Competing Interest

The authors declare that they have no known competing financial interests or personal relationships that could have appeared to influence the work reported in this paper.

CRediT authorship contribution statement

N. Rodríguez-Villagra: Conceptualization, Methodology, Validation, Investigation, Resources, Writing – original draft, Writing – review & editing, Visualization. **O. Riba:** Conceptualization, Methodology, Validation, Formal analysis, Writing – original draft, Writing – review & editing, Visualization. **A. Milena-Pérez:** Resources, Writing – review & editing. **J. Cobos:** Supervision, Funding acquisition. **L. Jimenez-Bonales:** Resources. **S. Fernández-Carretero:** Resources. **E. Coene:** Formal analysis, Writing – review & editing. **O. Silva:** Formal analysis, Writing – review & editing. **L. Duro:** Supervision, Funding acquisition, Project administration.

Acknowledgment

The research leading to these results has received funding from the European Commission Horizon 2020 Research and Training Programme of the European Atomic Energy Community (EURATOM) (H2020-NFRP-2016-2017-1) under Grant Agreement No. 755443 (DisCo project). The authors also want to thank to Sofía Durán and Luis Gutiérrez for their help in the samples analysis by ICP-MS and XRD, respectively.

References

[1] U.S. DOE, Roadmap: development of light water reactor fuels with enhanced accident tolerance. Report to congress., (2015), https://www.energy.gov/sites/default/files/2015/06/f23/Report%20to%20Congress%20-%20Accident%20Tolerant%20Fuels.pdf.
[2] , Accident tolerant fuel concepts for light water reactors, in: Proceedings of the Technical Meeting Held at Oak Ridge National Laboratories, United States Of America, 2016 13–16 October 2014IAEA-TECDOC-1797.
[3] OECD-NEA, State-of-the-art report on innovative fuels for advanced nuclear systems, Nuclear Science, NEA 6895 (2014), doi:10.1787/9789264248724-en.
[4] OCDE/NEA, State-of-the-art report on light water reactor accident-tolerant fuels, (2018), NEA 7317, https://www.oecd-nea.org/jcms/pl_15020/state-of-the-art-report-on-light-water-reactor-accident-tolerant-fuels?details=true.
[5] E. Hellestrand, Burnable poison reactivity control and other techniques to increase fuel burnup in LWR fuel cycles, Trans. Am. Nucl. Soc. 40 (1982) 181.
[6] W. Böhm, H.D. Kiehlmann, A. Nuefert, M. Peehs, Gd_2O_3 up to 9 weight percent, an established burnable poison for advanced fuel management in pressurized water reactors, Kerntechnik 50 (1987) 234–240.
[7] J. Arborelius, K. Backman, L. Hallstadius, M. Limback, J. Nilsson, B. Rebensdorff, G. Zhou, K. Kitano, R. Lofstrom, G. Ronnberg, Advanced doped UO_2 pellets in LWR applications, J. Nucl. Sci. Technol. 43 (9) (2006) 967–976.
[8] IAEAAdvanced Fuel Pellet Materials and Fuel Rod Design for Water Cooled Reactors, International Atomic Energy Agency, Vienna, 2010.
[9] S.M. Bragg-Sitton, M. Todosow, R. Montgomery, C.R. Stanek, R. Montgomery, W.J. Carmack, Metrics for the technical performance evaluation of light water reactor accident-tolerant fuel, Nucl. Technol. 195 (2) (2016) 111–123.
[10] H. He, P.G. Keech, M.E. Broczkowski, J.J. Noël, D.W. Shoesmith, Characterization of the influence of fission product doping on the anodic reactivity of uranium dioxide, Can. J. Chem. 85 (10) (2007) 702–713.
[11] M. Razdan, D.W. Shoesmith, Influence of trivalent-dopants on the structural and electrochemical properties of uranium dioxide (UO_2), J. Electrochem. Soc. 161 (3) (2013) 105–113.
[12] O. Roth, B. Kienzler, V. Metz, L. Duro, A. Valls, Leaching of high burn up spent fuel with and without matrix dopants, in: Proceedings of the Final (3rd) Annual Workshop Proceedings of the 7th EC FP CP FIRST-Nuclides Project, 2014, p. 2014.
[13] O. Roth, J. Low, K. Spahiu, Effects of matrix composition and sample preparation on instant release fractions from high burnup nuclear fuel, MRS Online Proc. Libr. 1665 (1) (2014) 261–266.
[14] O. Roth, J. Low, M. Granfors, K. Spahiu, Effects of matrix composition on instant release fractions from high burn-up nuclear fuel, MRS Proc. 1518 (2013) 145–150.
[15] K. Nilsson, O. Roth, M. Jonsson, Oxidative dissolution of ADOPT compared to standard UO_2 fuel, J. Nucl. Mater. 488 (2017) 123–128.
[16] DISCO, "Modern spent fuel dissolution and chemistry in failed container conditions" H2020-NFRP-2016-2017-1 Project ID: 755443. https://www.disco-h2020.eu/.
[17] M.M. Hossain, E. Ekeroth, M. Jonsson, Effects of HCO_3^- on the kinetics of UO_2 oxidation by H_2O_2, J. Nucl. Mater. 358 (2-3) (2006) 202–208.
[18] A. Milena-Pérez, L.J. Bonales, N. Rodríguez-Villagra, S. Fernández, V.G. Baonza, J. Cobos, Raman spectroscopy coupled to principal component analysis for studying UO_2 nuclear fuels with different grain sizes due to the chromia addition, J. Nucl. Mater. 543 (2021) 152581.2
[19] A. Nouri, P.D. Hodgson, C. Wen, Study on the role of stearic acid and ethylene-bis-stearamide on the mechanical alloying of a biomedical titanium based alloy, Metall. Mater. Trans. A 41 (6) (2010) 1409–1420.
[20] Y. Lin, K. Hwang, Effect of lubricant on powder properties and compacting performance of iron and stainless steel powders. I, Powder properties, J. Mater. Sci. Eng. 33 (4) (2001) 216–222.
[21] S. Fernandez, M.I. Nieto, J. Cobos, R. Moreno, CeO_2 pellet fabrication as spent fuel matrix analogue, J. Eur. Ceram. Soc. 36 (2016) 3505–3512.
[22] N. Rodriguez-Villagra, S. Fernandez, L.J. Bonales, A. Milena-Pérez, A. Núñez, S. Durán, L. Anta, L. Gutiérrez, J. Cobos, Production of unirradiated advanced doped UO_2 fuel for dissolution studies at repository conditions, in: Proceedings of the 3rd Annual Meeting Proceedings DisCo Project, 2020 (Grant Agreement: 755443).
[23] O. Riba, E. Coene, O. Silva, L. Duro, Spent fuel alteration model integrating processes of different time-scales, MRS Adv. 5 (3-4) (2020) 159–166.
[24] D.L. Parkhurst, C.A.J. Appelo, PHREEQC (version 3) – a computer program for speciation, batch-reaction, one-dimensional transport, and inverse geochemical calculations, in: U.S.G. Survey (Ed.) USGS, 2013.
[25] E. Giffaut, M. Grivé, P. Blanc, P. Vieillard, E. Colàs, H. Gailhanou, S. Gaboreau, N. Marty, B. Madé, L. Duro, Andra thermodynamic database for performance assessment: ThermoChimie, Appl. Geochem. 49 (2014) 225–236.
[26] M. Trummer, S. Nilsson, M. Jonsson, On the effects of fission product noble metal inclusions on the kinetics of radiation induced dissolution of spent nuclear fuel, J. Nucl. Mater. 378 (1) (2008) 55–59.
[27] E. Iglesias, J. Quiñones, Analogous materials for studying spent nuclear fuel: the influence of particle size distribution on the specific surface areaof irradiated nuclear fuel, Appl. Surf. Sci. 254 (2008) 6890–6896.
[28] N. Rodríguez-Villagra, U. Alonso, S. Durán, J.M. Cobo, L. Serrano, T. Missana, J. Cobos, Densidad de sitios superficiales y capacidad de sorción de la matriz de combustible irradiado, UO_2, (2016), Report Number DFN/RA-15/SP-16, http://documenta.ciemat.es/handle/123456789/1496.
[29] N. Rodríguez-Villagra, L. Serrano, S. Durán, J. Cobos, J. Quiñones, Estudios de alteración y modelación de la matriz del combustible nuclear irradiado en condiciones reductoras y a diferente fuerza iónica., (2017), Report Number DFN/RA-13/SP-17, http://documenta.ciemat.es/handle/123456789/1497.
[30] F. Clarens, J. de Pablo, I. Casas, J. Giménez, M. Rovira, Surface site densities of uranium oxides: UO_2, U_3O_8, in: V.M. Oversby, L.O. Werme (Eds.), Scientific Basis for Nuclear Waste Management XXVII, Materials Research Society, 2003, pp. 71–76.
[31] K. Kapoor, S.V. Ramana Rao, T.Sanyal Sheela, A. Singh, Study on solid solubility of Gd in UO_2 using X-ray diffraction, J. Nucl. Mater. 321 (2-3) (2003) 331–334.
[32] J.G. Kim, Y.K Ha, S.D Park, K.Y. Jee, W.H. Kim, Effect of a trivalent dopant, Gd^{3+}, on the oxidation of uranium dioxide, J. Nucl. Mater. 297 (3) (2001) 327–331.
[33] N. Liu, J. Kim, J. Lee, Y.S. Youn, J.G. Kim, J.Y. Kim, J.J. Noël, D.W. Shoesmith, Influence of Gd doping on the structure and electrochemical behavior of UO_2, Electrochim. Acta 247 (2017) 496–504.
[34] J.M. Elorrieta, L.J. Bonales, N. Rodriguez-Villagra, V.G. Baonza, J. Cobos, A detailed Raman and X-ray study of UO_{2+x} oxides and related structure transitions, Phys. Chem. Chem. Phys. 18 (2016) 28209–28216.
[35] J.M. Elorrieta, L.J. Bonales, S. Fernández, N. Rodríguez-Villagra, L. Gutiérrez-Nebot, V.G. Baonza, J. Cobos, Pre-and post-oxidation Raman analysis of (U, Ce)O_2 oxides, J. Nucl. Mater. 508 (2018) 116–122.
[36] American Society for Testing and Materials (ASTM) ASTM E112-13Standard test methods for determining average grain size, ASTM International, West Conshohocken, PA, USA, 2013.
[37] A. Rey, J. Giménez, I. Casas, F. Clarens, J. de Pablo, Secondary phase formation on UO_2 in phosphate media, Appl. Geochem. 23 (8) (2008) 2249–2255.
[38] I. Casas, J. Giménez, V. Martí, M.E. Torrero, J. de Pablo, Kinetic studies of unirradiated UO_2 dissolution under oxidizing conditions in batch and flow experiments, Radiochim. Acta 66/67 (1994) 23–27.
[39] R. Finch, R. Ewing, Uraninite alteration in an oxidizing environment and its relevance to the disposal of spent nuclear fuel, (1990), SKB Tech. Report No. TR 91-15.

[40] A. Martínez-Torrents, D. Serrano-Purroy, R. Sureda, I. Casas, J. de Pablo, Instant release fraction corrosion studies of commercial UO2 BWR spent nuclear fuel, J. Nucl. Mater. 488 (2017) 302–313.
[41] V.M. Oversby, V.M.O. Konsult, Uranium dioxide, SIMFUEL, and spent fuel dissolution rates - a review of published data, (1999), SKB Tech. Report No. TR 99-22.
[42] J. Bruno, E. Cera, J. de Pablo, L. Duro, S. Jordana, D. Savage, Determination of radionuclide solubility limits to be used in SR-97. Uncertainties associated to calculated solubilities, (1997) SKB Tech. Report No. TR 97-33.
[43] K. Ollila, L. Ahonen, Solubilities of uranium for HLA-99, (1998), POSIVA Tech. Report No. 98-13, http://www.iaea.org/inis/collection/NCLCollectionStore/_Public/30/013/30013965.pdf.
[44] W. Hummel, Solubility equilibria and geochemical modelling in the field of radioactive waste disposal, Pure Appl. Chem. 77 (2005) 631–641.
[45] R. Guillaumont, T. Fanghänel, J. Fuger, I. Grenthe, V. Neck, D.A. Palmer, M.H. Rand, Update on the Chemical Thermodynamics of Uranium, Neptunium, Plutonium, Americium and Technetium, Elsevier B.V., Amsterdam. Boston. Heilderberg. London, 2003 New York. Oxford. Paris. San Diego. San Francisco. Singapore. Sydney. Tokyo.
[46] V. Neck, J.I. Kim, Solubility and hydrolysis of tetravalent actinides, Radiochim. Acta 89 (2001) 1–16.
[47] T. Yajima, Y. Kawamura, S. Ueta, Uranium(IV) solubility and hydrolysis constants under reduced conditions, Mater. Res. Soc. Symp. Proc. 353 (1995) 1137.
[48] D. Rai, A.R. Felmy, J.L. Ryan, Uranium (IV) hydrolysis constants and solubility products of $UO_2 \cdot xH_2O$ (am), Inorg. Chem. 29 (1990) 260–264.
[49] M.E. Broczkowski, J.J. Noel, D.W. Shoesmith, The inhibiting effects of hydrogen on the corrosion of uranium dioxide under nuclear waste disposal conditions, J. Nucl. Mater. 346 (1) (2005) 16–23.
[50] M.E. Broczkowski, J.J. Noel, D.W. Shoesmith, The influence of dissolved hydrogen on the surface composition of doped uranium dioxide under aqueous corrosion conditions, J. Electroanal. Chem. 602 (1) (2007) 8–16.
[51] A.D. Apte, V. Tare, P. Bose, Extent of oxidation of Cr(III) to Cr(VI) under various conditions pertaining to natural environment, J. Hazard. Mater. 128 (2) (2006) 164–174.
[52] N. Unceta, F. Séby, J. Malherbe, O.F.X. Donard, Chromium speciation in solid matrices and regulation: a review, Anal. Bioanal.Chem. 397 (3) (2010) 1097–1111.
[53] D. Rai, B.M. Sass, D.A. Moore, Chromium(III) hydrolysis constants and solubility of chromium(III) hydroxide, Inorg. Chem. 26 (3) (1987) 345–349.
[54] S. Brunauer, P. Emmet, E. Teller, Adsorption of Gases in Multimolecular Layers, J. Am. Chem. Soc. 60 (1938) 309, doi:10.1021/ja01269a023.
[55] P. Carbol, P. Fors, T. Gouder, K. Spahiu, Hydrogen suppresses UO2 corrosion, Geochim. Cosmochim. Acta 73 (15) (2009) 4366–4375.
[56] M. Trummer, M. Jonsson, Resolving the H_2 effect on radiation induced dissolution of UO_2-based spent nuclear fuel, J. Nucl. Mater. 396 (2010) 163–169.
[57] K. Ollila, Influence of radiolysis on UO2 fuel matrix dissolution under disposal conditions literature study, (2011), POSIVA Tech. Report No. 2011-27, http://inis.iaea.org/search/search.aspx?orig_q=RN:43066688.
[58] M. Cherian, M.S. Rao, W.T. Yang, J.M. Jehng, A.M. Hirt, G. Deo, Oxidative dehydrogenation of propane over Cr_2O_3/Al_2O_3 and Cr_2O_3 catalysts: effects of loading, precursor and surface area, Appl. Catal. A Gen. 233 (1) (2002) 21–33.
[59] B.Y. Jibril, N.O. Elbashir, S.M. Al-Zahrani, A.E. Abasaeed, Oxidative dehydrogenation of isobutane on chromium oxide-based catalyst, Chem. Eng. Process. Process Intensif. 44 (8) (2005) 835–840.
[60] E. Romero, J.C. Rodríguez, J.A. Peña, A. Monzón, Coking kinetics of a Cr_2O_3/Al_2O_3 catalyst during 1-butene dehydrogenation: effect of H_2 partial pressure, Can. J. Chem. Eng. 74 (6) (1996) 1034–1038.
[61] J.R. Sohn, S.G. Ryu, Surface characterization of chromium oxide-zirconia catalyst, Langmuir 9 (1) (1993) 126–131.
[62] U. Scharf, H. Schneider, A. Baiker, A. Wokaun, Chromia supported on titania. III. structure and spectroscopic properties, J. Catal. 145 (2) (1994) 464–478.
[63] W.K. Jóźwiak, I.G. Dalla Lana, Interactions between the chromium oxide phase and support surface; redispersion of α-chromia on silica, alumina and magnesia, J. Chem. Soc. Faraday Trans. 93 (15) (1997) 2583–2589.
[64] M.I. Zaki, M.A. Hasan, N.E. Fouad, Stability of surface chromate–A physicochemical investigation in relevance to environmental reservations about calcined chromia catalysts, Appl. Catal. A Gen. 171 (2) (1998) 315–324.